ANZIAM J. 59(2018), 281–292
doi:10.1017/S1446181117000426

MODELLING HYDROGEN CLEARANCE FROM THE RETINA

D. E. FARROW[✉1], G. C. HOCKING[1], S. J. CRINGLE[2] and D.-Y. YU[2]

(Received 16 November, 2016; accepted 29 September, 2017; first published online 25 January 2018)

Abstract

The human retina is supplied by two vascular systems: the highly vascular choroidal, situated behind the retina; and the retinal, which is dependent on the restriction that the light path must be minimally disrupted. Between these two circulations, the avascular retinal layers depend on diffusion of metabolites through the tissue. Oxygen supply to these layers may be threatened by diseases affecting microvasculature, for example diabetes and hypertension, which may ultimately cause loss of sight.

An accurate model of retinal blood flow will therefore facilitate the study of retinal oxygen supply and, hence, the complications caused by systemic vascular disease. Here, two simple models of the blood flow and exchange of hydrogen with the retina are presented and compared qualitatively with data obtained from experimental measurements. The models capture some interesting features of the exchange and highlight effects that will need to be considered in a more sophisticated model and in the interpretation of experimental results.

2010 *Mathematics subject classification*: 92C50.

Keywords and phrases: mathematical model, hydrogen clearance, advection/diffusion.

1. Introduction

The exchange of metabolites between the blood and retina is very important in the health of the eye and also in vision. Part of understanding this process is to determine accurately the blood flow in the eye and near the retina in particular. There are many problems inherent in determining this, not the least of which is a means of extracting reliable data.

The eye consists of several layers that work together to provide optical input to the brain. The outer layer is called the sclera (the white of the eye). Just inside this is the choroid, which is a layer of dense vasculature that provides a conduit for oxygen and

[1]Mathematics and Statistics, Murdoch University, Murdoch WA 6150, Australia; e-mail: d.farrow@murdoch.edu.au, g.hocking@murdoch.edu.au.
[2]Lions Eye Institute, 2 Verdun St, Nedlands WA 6009, Australia; e-mail: Steve@lei.org.au, dyyu@lei.org.au.

other chemicals [10]. The choroidal circulation is a very dense mesh of large-diameter capillaries, lying directly behind the retina. Between this and the retina, there is the tough highly elastic Bruch's membrane. Approximately 80% of the total blood flow occurs in the choroid. The avascular retinal region is adjacent to this, and then there is the vascular region (which is roughly half the total retinal width). This comprises much smaller capillaries, separated by tissue, such that the blood flow is an order of magnitude lower than in the choroid. The retina is light sensitive and forms the innermost layer on the back of the eye. Retinal ganglion cells near the surface send information to the brain via the optic nerve. The choroidal and retinal layers are very thin, making up no more than several hundred microns. Blood is supplied to the eye via the ophthalmic artery, situated nearly centrally at the back of the eye, and departs via the central retinal vein, which runs parallel to the artery.

One experimental procedure used to determine the blood flow is the hydrogen clearance technique, in which a bolus of hydrogen-saturated saline solution is introduced to the blood supply and then measured across the retina [1, 11]. This method was found to give highly reproducible concentration traces. Hydrogen is a conservative tracer and the subsequent decay of the hydrogen concentration may be used to estimate the blood flow.

The principles of hydrogen washout to estimate tissue blood flow were described by Kety [7]. The technique is based upon the detection and rate of clearance of hydrogen from the tissue under investigation. Under ideal conditions, the clearance rate is directly proportional to the local blood flow per unit weight of tissue. However, the theoretical requirements cannot be met in the eye. The "ideal" condition requires that the measurements should be made in a uniformly perfused three-dimensional tissue. This situation cannot be guaranteed in the eye, due to the necessarily short duration of the hydrogen-saturated saline injection. Also, the inhomogeneous circulations on either side of the avascular retinal tissue depart from the ideal. Hence, a mathematical model of the hydrogen clearance through the retina should help to confirm or refute blood flow estimates and also estimate other parameters, for example diffusivity.

Apart from making the "hydrogen clearance curves" difficult to interpret unambiguously, the inhomogeneities in the anatomy of the posterior segment of the eye introduce complexity into the modelling of the problem. For this reason, we make a start by considering two simple models of the retinal blood supply and examine their behaviour in the light of experimental results. The study is by no means comprehensive, but does provide some interesting results that need to be considered in any future interpretation of data.

There has been extensive modelling of blood flow in the retina and surrounding ocular region, and also of the interactions of oxygen and metabolites with the surrounding tissue. A detailed review of some of these models was given by Arciero et al. [2]. The focus of many of these models is the actual flow of blood in the micro-arteries and the changes due to the intra-ocular pressure. This allows analysis of the direct conditions that cause diseases such as glaucoma and macular degeneration, and are pivotal in the symptoms of diabetes. The models range from models that simulate

https://doi.org/10.1017/S1446181117000426 Published online by Cambridge University Press

the flow using an electric circuit analogue [6] to direct computational simulation of flow in the blood vessels [9]. Friedland [3] proposed a model of oxygen transport in the retina and Goldman [5] gave a summary of models of oxygen transport within the microvasculature.

In general, these models are trying to generate a detailed mapping of flow and infusion within a retinal landscape. In this paper, we are taking a slightly broader view, panning back to consider the general interchange between the choroidal circulation and the avascular retina. By considering this higher level focus, we can obtain a big picture view of interchange between a conservative tracer in the blood and in the retinal tissue without the confusion of the complicated geometry. This focus allows us to consider the simple interaction between the blood flow and surrounding tissue, and shows some very interesting effects that are obscured by the details of the more sophisticated models. It also provides some guidelines for determining general blood flow using the hydrogen clearance technique, or for monitoring the passage of the bolus of hydrogen (or perhaps an injected drug) through the retinal system.

For the purposes of the model, it is assumed that the blood flow in the vessels is laminar, with a negligible pulsatile component [4]. Thus, the rapid diffusion of hydrogen through the retina must be modelled, relating the retinal circulation to the more dominant source of hydrogen in the choroid. The models presented below only consider the choroidal blood supply, as the retinal blood supply is an order of magnitude smaller.

2. Two-layer model

The choroid and avascular retina are modelled as two well-mixed layers. The blood flow in the choroid is assumed to be moving at constant and uniform speed U_0. This assumption is based on the highly vascular nature of the choroid, so that on average the flow will be uniform through this region (rather than simulating a series of micro-arteries individually). There is an exchange of hydrogen between the layers that is proportional to the difference in their concentration values at a rate λ. The concentrations in the two layers are given by $C(x,t)$ in the moving layer (choroid) and $R(x,t)$ in the stationary layer (avascular retina). The model equations are

$$\frac{\partial C}{\partial t} + U_0 \frac{\partial C}{\partial x} = -\lambda(C - R),$$
$$\frac{\partial R}{\partial t} = \lambda(C - R)$$

and the initial conditions are $C(x,0) = C_0(x)$ and $R(x,0) = 0$. The idea here is that there is some locally nonzero concentration of hydrogen in the choroid which is then advected along the choroid, while at the same time there is an exchange between the layers.

The equations are first nondimensionalized using $x \sim l$, where l is the length scale associated with the initial distribution $C_0(x)$ and $t \sim l/U_0$. Both C and R are

https://doi.org/10.1017/S1446181117000426 Published online by Cambridge University Press

nondimensionalized using a typical value from C_0. The equations become

$$\frac{\partial C}{\partial t} + \frac{\partial C}{\partial x} = -\alpha(C - R), \tag{2.1}$$

$$\frac{\partial R}{\partial t} = \alpha(C - R), \tag{2.2}$$

where all variables are now nondimensional, and $\alpha = l\lambda/U_0$ is a dimensionless exchange parameter.

We first consider the periodic case where the initial conditions are $C(x, 0) = C_0(x)$ and $R(x, 0) = 0$ for $x \in [0, L]$, and the solution is assumed to have period L. The model above can then be solved by writing the dependent variables as a complex Fourier series

$$C(x,t) = \sum_{k=-\infty}^{\infty} C_k(t) \exp(2\pi i k x/L), \quad R(x,t) = \sum_{k=-\infty}^{\infty} R_k(t) \exp(2\pi i k x/L).$$

Substitution and equating of coefficients yield a system of linear ordinary differential equations (ODEs) for C_k and R_k given by

$$\frac{dC_k}{dt} = -(\alpha + 2\pi i k/L)C_k + \alpha R_k,$$

$$\frac{dR_k}{dt} = \alpha C_k - \alpha R_k$$

for $k \in Z$. Solving this system and applying the $R(x, 0) = 0$ condition yields the general solutions

$$C(x,t) = \sum_{k=-\infty}^{\infty} A_k[(\alpha + \lambda_{1k})e^{\lambda_{1k}t} - (\alpha + \lambda_{2k})e^{\lambda_{2k}t}] \exp(2k\pi i x/L), \tag{2.3}$$

$$R(x,t) = \alpha \sum_{k=-\infty}^{\infty} A_k[e^{\lambda_{1k}t} - e^{\lambda_{2k}t}] \exp(2k\pi i x/L), \tag{2.4}$$

where

$$\lambda_{1k} = -(\alpha + i\pi k/L) - \sqrt{\alpha^2 - \pi^2 k^2/L^2} \quad \text{and} \quad \lambda_{2k} = -(\alpha + i\pi k/L) + \sqrt{\alpha^2 - \pi^2 k^2/L^2}.$$

The constants A_k are determined by the initial condition $C(x, 0) = C_0(x)$.

By taking the limit as $L \to \infty$ in (2.3) and (2.4) in the usual way, the Fourier series solution can be converted to a Fourier transform solution

$$C(x,t) = \int_{-\infty}^{\infty} A(\omega)[(\alpha + \lambda_1(\omega))e^{\lambda_1(\omega)t} - (\alpha + \lambda_2(\omega))e^{\lambda_2(\omega)t}]e^{2\pi i\omega x}\, d\omega$$

and

$$R(x,t) = \alpha \int_{-\infty}^{\infty} A(\omega)[e^{\lambda_1(\omega)t} - e^{\lambda_2(\omega)t}]e^{2\pi i\omega x}\, d\omega,$$

https://doi.org/10.1017/S1446181117000426 Published online by Cambridge University Press

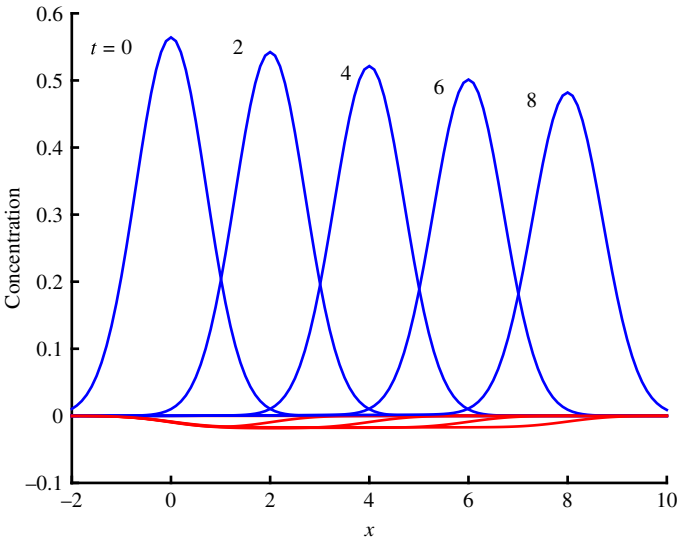

FIGURE 1. Profiles of $C(x,t)$ (blue online) and $-R(x,t)$ (red online) at times $t = 0, 2, 4, 6, 8$ for $\alpha = 0.02$. The profiles for $-R$ appear below the x-axis to improve clarity.

where

$$\lambda_1(\omega) = -\alpha - i\pi\omega + \sqrt{\alpha^2 - \pi^2\omega^2}, \quad \lambda_2(\omega) = -\alpha - i\pi\omega - \sqrt{\alpha^2 - \pi^2\omega^2}$$

and $A(\omega)$ is given by

$$A(\omega) = \frac{1}{2\sqrt{\alpha^2 - \pi^2\omega^2}} \int_{-\infty}^{\infty} C_0(x) e^{-2\pi i\omega x}\, dx.$$

It only remains to specify the initial distribution of hydrogen in the choroid. A natural choice is the Gaussian profile $C_0 = e^{-x^2}/\sqrt{\pi}$ (so that $\int_{-\infty}^{\infty} C_0(x)\, dx = 1$), in which case the solutions are

$$C(x,t) = \int_{-\infty}^{\infty} \frac{e^{-\pi^2\omega^2}}{2\sqrt{\alpha^2 - \pi^2\omega^2}} [(\alpha + \lambda_1(\omega))e^{\lambda_1(\omega)t} - (\alpha + \lambda_2(\omega))e^{\lambda_2(\omega)t}] e^{2\pi i\omega x}\, d\omega$$

and

$$R(x,t) = \alpha \int_{-\infty}^{\infty} \frac{e^{-\pi^2\omega^2}}{2\sqrt{\alpha^2 - \pi^2\omega^2}} [e^{\lambda_1(\omega)t} - e^{\lambda_2(\omega)t}] e^{2\pi i\omega x}\, d\omega.$$

Figure 1 shows a series of profiles of C and R at various times for $\alpha = 0.02$. For this low value of α there is little exchange between the two layers. The initial profile is advected with barely any change in shape at speed 1, with its magnitude slowly decreasing as hydrogen slowly diffuses from the choroid to the retina. In fact, for the times shown in Figure 1, the solution for $C(x,t)$ is well approximated by $C(x,t) = C_0(x-t)e^{-\alpha t}$, which can be obtained from (2.1) by assuming $R \equiv 0$.

https://doi.org/10.1017/S1446181117000426 Published online by Cambridge University Press

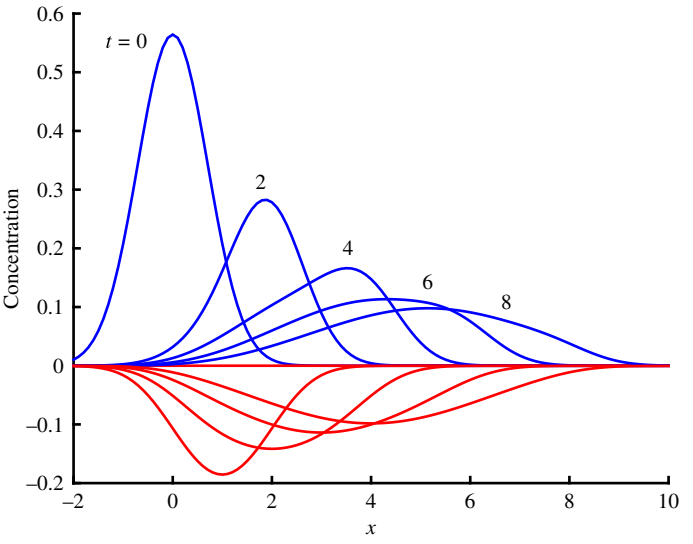

FIGURE 2. Profiles of $C(x,t)$ (blue online) and $-R(x,t)$ (red online) at times $t = 0, 2, 4, 6, 8$ for $\alpha = 0.5$. The profiles for $-R$ appear below the x-axis to improve clarity.

After the bolus of hydrogen has moved further than its initial width, hydrogen begins to diffuse back from the retina into the choroid. This leads to the original symmetry of the hydrogen distribution in the choroid breaking down. In Figure 1 this is barely visible as a slight thickening of the left-hand tail for later times.

Figure 2 shows a similar set of profiles but for $\alpha = 0.5$. For this value of α, there is a much stronger exchange of hydrogen between the choroid and retina. The magnitude of the original distribution of hydrogen rapidly decreases, and the original symmetry of the hydrogen distribution is soon lost as hydrogen that has diffused into the retina at earlier times diffuses back into the choroid as the bolus moves through. This process of early diffusion of hydrogen into the retina, and then diffusion back into the choroid, leads to the peak concentration in the retina lagging the peak in the choroid. Also, after some time, there is an approximately equal amount of hydrogen in both the choroid and the retina. Defining

$$\bar{C}(t) = \int_{-\infty}^{\infty} C(x,t)\,dx \quad \text{and} \quad \bar{R}(t) = \int_{-\infty}^{\infty} R(x,t)\,dx,$$

and using (2.1) and (2.2) (with $\bar{C}(0) = 1$ and $\bar{R}(0) = 0$), it can be shown that

$$\bar{C}(t) = \tfrac{1}{2}(1 + e^{-2\alpha t}) \quad \text{and} \quad \bar{R}(t) = \tfrac{1}{2}(1 - e^{-2\alpha t}). \tag{2.5}$$

It follows from (2.5) that as $t \to \infty$, the total amount of hydrogen is evenly split between the choroid and retina. By $t = 8$, the profiles in Figure 2 have very close to equal quantities in both the choroid and the retina. For later times, the profiles evolve by stretching out horizontally and lowering their peak value.

https://doi.org/10.1017/S1446181117000426 Published online by Cambridge University Press

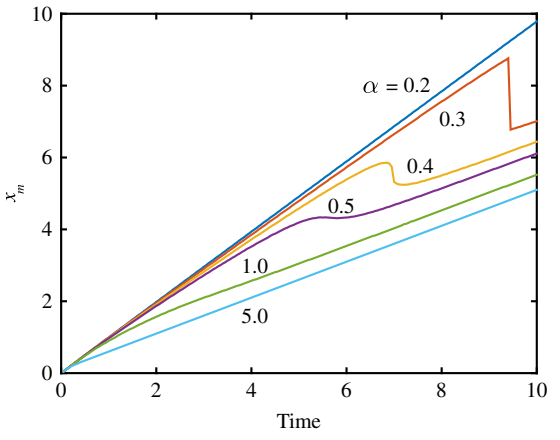

FIGURE 3. The x-location of maximum $C(x, t)$, x_m, as a function of t for various values of α. Note that for $\alpha = 0.3$ there is a discontinuity at $t \approx 9.5$.

Less obvious from Figure 2 is that for later times the peak concentration in the choroid is travelling at a slower speed than that set by the advection velocity in the choroid. In particular, the peak concentration at $t = 8$ is located at $x \approx 5.5$, whereas under pure advection it would be at $x = 8$. Close tracking of the peak concentration location shows that for $t > 8$ the profiles in Figure 2 travel at speed 0.5.

Figure 3 shows the location $x_m(t)$ of the peak concentration in the choroid for various values of α. For each value of α, there is a period for $t > 0$ where the peak is travelling at a speed close to the advection velocity 1. At some time later (that depends on α), there is a shift to a lower speed, which is one-half of the advection speed in the choroid. For small values of α this transition happens later and more abruptly. In fact, from Figure 3 there is a discontinuity at the transition point for $\alpha = 0.3$ (which occurs at $t \approx 9.5$). This discontinuity is caused by the shift from the location of the peak being set by the advected peak of the initial distribution to the peak generated by diffusion back into the choroid from the retina. The latter peak travels at half the advection speed in the choroid. Figure 4 shows a series of profiles for $\alpha = 0.3$ during the period that the transition occurs. The peak associated with the original distribution is visible at $t = 6, 8$ and 10, but has all but disappeared by $t = 12$. The jump from one peak to the other occurs between $t = 8$ and 10 as indicated by Figure 3.

In the experimental situation, hydrogen concentration measurements consist of time series at specific locations. The experimental time series are characterized by an initial rapid rise to a maximum value and a slow tailing-off. Figure 5 shows a number of time series at different x-locations for $\alpha = 0.5$ taken from the model results. All the time series show qualitatively the same behaviour as the experimental results. There is a relatively rapid rise to the maximum value followed by a more gradual decay. The mechanism that generates the relatively slow decay in these cases follows from the discussion above. Once the profiles have moved into the slower propagation phase

https://doi.org/10.1017/S1446181117000426 Published online by Cambridge University Press

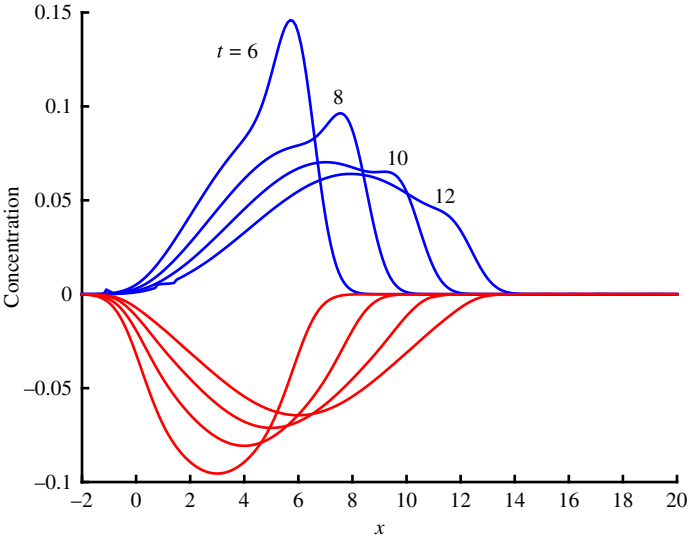

FIGURE 4. Profiles of $C(x,t)$ (blue online) and $-R(x,t)$ (red online) at times $t = 6, 8, 10, 12$ for $\alpha = 0.3$ showing the emergence of a new peak value behind the peak associated with the original distribution. The profiles for $-R$ appear below the x-axis to improve clarity.

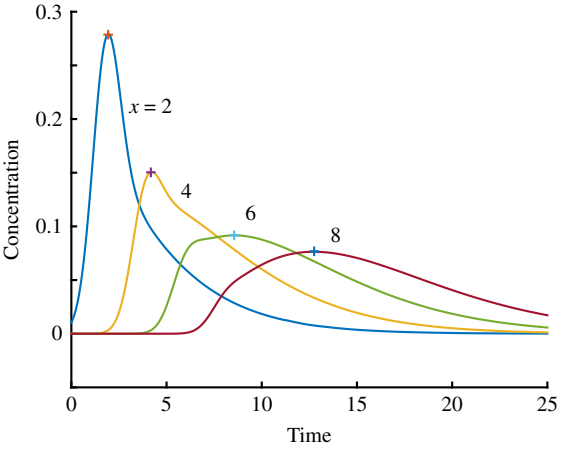

FIGURE 5. Time series of choroidal hydrogen concentration $C(x,t)$ at locations $x = 2, 4, 6, 8$ for $\alpha = 0.5$ taken from the model results. The "+" indicates the peak value for each series.

(which happens at $t \approx 7$ for $\alpha = 0.5$), the profile in the choroid maintains more or less the same shape, but elongates and flattens as time progresses. The leading edge of the distribution travels at speed 1, but the peak value (which is decreasing in magnitude with time) travels at half of that speed. Of particular note is that the arrival time of the peak concentration at a particular location cannot generally be used to calculate the speed of the choroidal blood flow. From Figure 5 the peaks at $x = 2$ and $x = 4$

https://doi.org/10.1017/S1446181117000426 Published online by Cambridge University Press

correspond fairly closely to the expected times, but the peaks at $x = 6$ and $x = 8$ are significantly delayed. This is because at these later times the peak concentration no longer corresponds to the advection of the peak in the initial concentration profile.

3. 2-D advection/diffusion model

The model described in the previous section is a relatively crude representation of the choroid/retina system. In this section, a fully two-dimensional (2-D) model is formulated that includes transport via diffusion across, as well as along, the choroidal and retinal layers.

The choroid/retina system is modelled as a rectangular region $x \in (0, L)$, $z \in (-D, 0)$ within which the evolving hydrogen concentration is governed by the advection–diffusion equation

$$\frac{\partial C}{\partial t} + U(z)\frac{\partial C}{\partial x} = \frac{1}{Pe}\left(\frac{\partial^2 C}{\partial x^2} + \frac{\partial^2 C}{\partial z^2}\right), \tag{3.1}$$

where $C(x, z, t)$ is the hydrogen concentration in the choroid/retina system, $Pe = U_0 l/\kappa$ is the Péclet number and κ is the diffusivity of hydrogen in the eye tissue. The (dimensionless) velocity profile $U(z)$ takes the form

$$U(z) = \begin{cases} 1 & -T < z < 0, \\ 0 & -D < z < -T, \end{cases}$$

where $T < D$ is the thickness of the choroid in dimensionless terms. Thus, in this model, the choroid occupies the layer $-T < z < 0$ and the retina occupies $-D < z < -T$.

The model is closed by adding boundary conditions to (3.1). Periodicity is assumed in the x-direction, and zero-flux boundary conditions are applied at $z = 0$ and $z = -D$. The initial condition consists of a sine-profile bolus of hydrogen in the choroid

$$C(x, z, 0) = \begin{cases} -\sin(2\pi x)\sin(2\pi z/T) & 0 < x < 1, -T < z < 0, \\ 0 & \text{otherwise.} \end{cases}$$

The above model is solved numerically in the following way. All spatial derivatives are replaced by a finite-volume representation. For the advective terms, quadratic upwinding is used [8]. For the diffusion terms, a standard centred difference is used. This leads to a large set of ODEs which are solved using `ode45` in MATLAB. In the simulations here $L = 10$, $D = 2$ and $T = 1$. The discretization has $I = 100$ points in the horizontal and $J = 50$ in the vertical.

Several simulations for different values of Pe have been carried out, and only a subset is presented here. In this 2-D model, Pe qualitatively acts like the inverse of the interaction parameter α in the two-layer model above.

Figure 6 shows contours of the distribution of C for three different times in the choroid/retina system, including the initial distribution, for $Pe = 16$. For this value of Pe, the advection in the choroid dominates the evolution of C in the choroid/retina system. This case is analogous to the low-α case for the well-mixed

https://doi.org/10.1017/S1446181117000426 Published online by Cambridge University Press

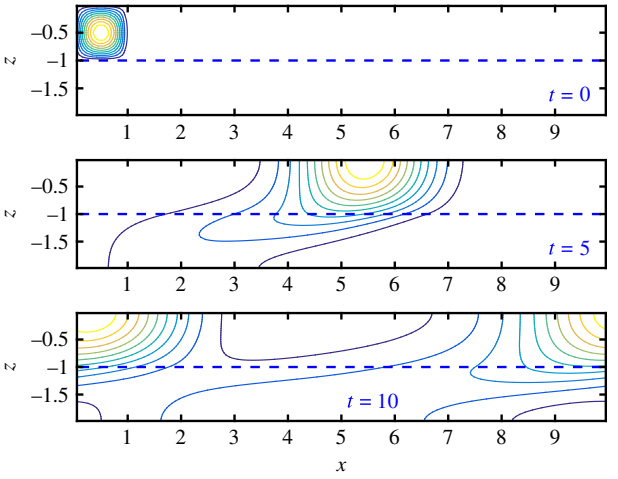

FIGURE 6. Contours of hydrogen concentration for $t = 0, 5$ and 10 for $Pe = 16$. The dashed line indicates the boundary between the choroid and retina.

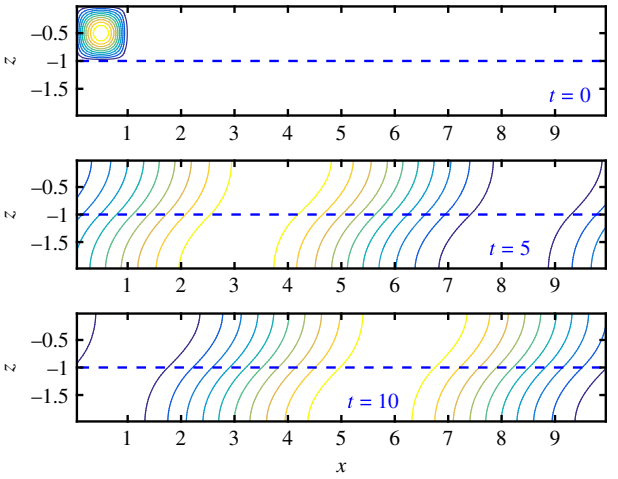

FIGURE 7. Contours of hydrogen concentration for $t = 0, 5$ and 10 for $Pe = 2$. The dashed line indicates the boundary between the choroid and retina.

model considered earlier. Diffusion dominates for small times ($t < 1$) with the initially sharp gradients rapidly being smoothed out. After this the bolus moves through the choroid with relatively little change in form. By $t = 10$ the centre of mass of the bolus has travelled nearly the entire length of the domain indicating that advection is the dominant transport mechanism. There has been some diffusion of hydrogen into the retina but the bulk remains in the choroid. By the end of the simulation at $t = 10$ most of the hydrogen remains in the choroid.

Figure 7 shows similar contour plots to Figure 6 but with $Pe = 2$. For this value of Pe, diffusion plays a much more dominant role in the transport of hydrogen,

https://doi.org/10.1017/S1446181117000426 Published online by Cambridge University Press

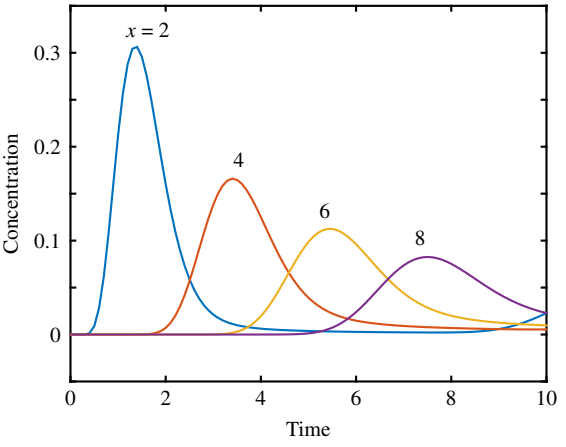

FIGURE 8. Time series of hydrogen concentration in the middle of the choroid at $x = 2, 4, 6$ and 8 for $Pe = 16$.

particularly with greater exchange between the choroidal and retinal layers. By $t = 5$, the distribution of hydrogen in the two layers has a clear symmetry with approximately equal amounts in each layer that is apparently maintained at least up to $t = 10$. This is very similar to the high-interaction case for the two-layer model above, although there is some cross-layer structure that could not be captured by the earlier model. Note also that at $t = 10$, the highest concentration of hydrogen in the flowing layer occurs at $x \approx 6$. Under pure advection, this highest concentration would be expected to occur at $x \approx 10$. This reduced apparent advection speed is also observed in the high-interaction case of the earlier two-layer model.

Figure 8 shows a number of time series of the hydrogen concentration within the flowing layer at various x-locations. Each of these time series reproduces qualitatively experimental observations with an initial rise in hydrogen concentration followed by a relatively slow decay back to zero.

4. Concluding remarks

This paper has developed two simple models for the transport of hydrogen in the retina. The models are motivated by experiments on hydrogen clearance within a rat's retina, which in turn are used for estimating blood flow in the eye. Despite their simplicity, the models are able to qualitatively reproduce experimental observations; specifically, the rapid rise and relatively gentle fall in the time series of hydrogen concentration at fixed locations. The models provide an explanation for this observation in terms of the diffusion of hydrogen from the retina back into the choroid, once the injected bolus of hydrogen is carried through the choroid. An interesting feature of this exchange process is that it leads to an apparently reduced advection velocity. The speed of the location of peak hydrogen concentration in the

https://doi.org/10.1017/S1446181117000426 Published online by Cambridge University Press

flowing choroid does not generally correspond to that predicted by the speed of the underlying flow.

There are many features of blood flow in the eye that have been omitted from the present models that are avenues for further work. These include adding additional layers (for example, vascular retina, sclera etc), accounting for geometrical features (curvature and changing thickness) and more accurate modelling of flow and transport within and between the physiological components of the eye.

References

[1] V. A. Alder, D. Y. Yu, S. J. Cringle and E. N. Su, "Experimental approaches to diabetic retinopathy", *Asia-Pac. J. Ophthalmol.* **4** (1992) 20–25; http://research-repository.uwa.edu.au/en/publications/experimental-approaches-to-diabetic-retinopathy(a439eaca-237f-423f-874d-19f00138b070).html.

[2] J. C. Arciero, P. Causin and F. Malgoroli, "Mathematical methods for modeling the microcirculation", *AIMS Biophys.* **4** (2017) 362–399; doi:10.3934/biophy.2017.3.362.

[3] A. B. Friedland, "A mathematical model of transmural transport of oxygen to the retina", *Bull. Math. Biol.* **40** (1978) 823–837; doi:10.1007/BF02460609.

[4] E. Friedman, T. R. Smith and T. Kuwabara, "Retinal microcirculation *in vivo*", *Invest. Ophthalmol. Vis. Sci.* **3** (1964) 217–226; http://iovs.arvojournals.org/article.aspx?articleid=2203699.

[5] D. Goldman, "Theoretical models of microvascular oxygen transport to tissue", *Microcirculation* **15** (2008) 795–811; doi:10.1080/10739680801938289.

[6] G. Guidoboni, A. Harris, S. Cassani, J. Arciero, B. Siesky, A. Amireskandari, L. Tobe, P. Egan, I. Januleviciene and J. Park, "Intraocular pressure, blood pressure and retinal blood flow autoregulation: a mathematical model to clarify their relationship and clinical relevance", *Invest. Ophthalmol. Vis. Sci.* **55** (2014) 4105–4118; doi:10.1167/iovs.13-13611.

[7] S. S. Kety, "The theory and applications of the exchange of inert gas at the lungs and tissues", *Pharmacol. Rev.* **3** (1951) 1–41; http://pharmrev.aspetjournals.org/content/3/1/1.

[8] B. P. Leonard, "A stable and accurate convective modelling procedure based on quadratic upstream interpolation", *Comput. Methods Appl. Mech. Engrg.* **19** (1979) 59–98; doi:10.1016/0045-7825(79)90034-3.

[9] T. W. Secomb, "Blood flow in the microcirculation", *Annu. Rev. Fluid Mech.* **49** (2017) 443–461; doi:10.1146/annurev-fluid-010816-060302.

[10] G. A. Winchell, "Mathematical model of inert gas washout from the retina: evaluation of hydrogen washout as a means of determining retinal blood flow in the cat", Master's Thesis, Northwestern University, Evanston, USA, 1983; https://books.google.com.au/books?id=CAKoGwAACAAJ.

[11] D. Y. Yu, V. A. Alder and S. J. Cringle, "Measurement of blood flow in rat eyes by hydrogen clearance", *Amer. J. Physiol. (Heart Circ. Physiol.)* **261**(30) (1991) H960–H968; https://www.ncbi.nlm.nih.gov/pubmed/1887939.